Proceedings of the NROCK 2023
The IV Nordic Symposium on
Rock Mechanics and Rock Engineering
ISBN 978-9935-9436-2-0
DOI 10.33112/nrock2023.13

Large-scale laboratory model tests simulating rock mass uplift failure

Bjarte Grindheim (bjarte.grindheim@ntnu.no)

B. Grindheim, C. C. Li
Department of Geoscience and Petroleum, Norwegian University of Science and Technology (NTNU), Trondheim, Norway
A. H. Høien
Norwegian Public Roads Administration (NPRA), Bergen, Norway

ABSTRACT

Rock anchors are high-capacity reinforcement measures used to stabilise large-scale infrastructure. There are four main failure mechanisms for rock anchors, which are: (1) rock mass uplift failure; (2) grout-rock interface failure; (3) tendon-grout interface failure; and (4) steel tendon tensile failure. A large-scale laboratory test rig has been developed to test block models which simulates rock mass uplift failure (failure mode 1). The design methods against failure mode 1 are the most conservative and least satisfactory design methods according to literature. The full-field displacements of the models were monitored with digital image correlation (DIC). The block model tests had higher capacities than what was calculated with the current design methods using the weight of overlying rock cone and presumptive shear strength values along the assumed failure cone. The capacity and failure shape in the block models showed to be structurally dependent on the block model pattern. The horizontal stress in the models increased during the tests, which showed that load arches were induced in the block models during the uplift. The load capacity of the block models increased with model height and horizontal stress level.

KEYWORDS

Block model, anchor pullout, load arching, failure mode, influence of joint pattern.

INTRODUCTION

Rock anchors has been used as load carrying elements for large-scale infrastructures since the first-time usage on Cheurfas dam in Algeria in 1934 (Merrifield et al., 2013). Later, the usage has been expanded to stabilisation of bridges (Schlotfeldt et al., 2013), wind turbines (Shabanimashcool et al., 2018), slopes (Choi et al., 2013), stadiums (Jordan, 2007), large statues (Koca et al., 2011), reinforcement of underground caverns (Aoki, 2007), and anchorage of submerged buildings (Roesen and Trankjær, 2021) and tunnels (Mothersille and Littlejohn, 2012). The loads from the structures are transferred to the stable rock ground by rock anchors. The anchor is loaded in tension, and it transfers the structural load to the stable rock through shear stresses along the two surfaces tendon-grout and grout-rock (Brown, 2015).

According to literature can a rock anchor fail in one of four principal ways (Littlejohn and Bruce, 1977; Brown, 2015). These are (1) rock mass uplift failure, (2) grout-rock interface failure, (3) tendon-grout interface failure, and (4) tensile failure of the anchor steel. The failure modes are showed in Figure 1. The capacity of an anchor is equal to the failure mode with the lowest capacity (Brown, 2015). The capacity of the failure modes 2-4 are calculated for individual anchors, while for failure mode 1 the interaction between adjacent anchors must be considered if they are installed in close vicinity (Brown, 2015).

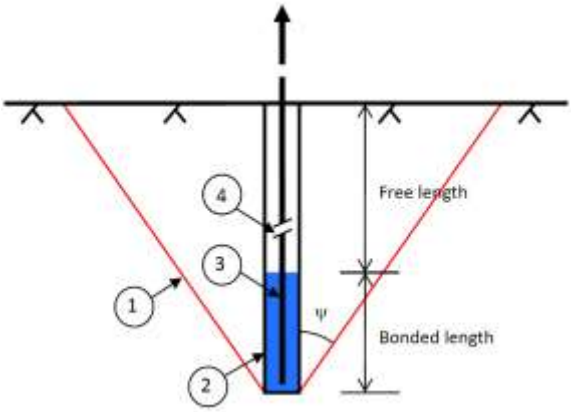

Figure 1. Grouted rock anchors can in principle fail in four ways: (1) rock mass uplift failure; (2) grout-rock bond or interface failure; (3) tendon-grout bond or interface failure; and (4) steel tendon tensile failure.

Brown (2015) carried out a thorough review on the design of rock anchors. In the review, it was concluded that the design against failure mode 1, failure of the rock mass from uplift, was based upon simplified assumptions on the stress distribution and volume of rock mass influenced, which has resulted in a design method that is excessively conservative and represents poor engineering practice. To make a precise design of rock anchors, it is required to understand the mechanisms and interaction between the anchor and the rock mass (Showkati et al., 2015). To improve the design of rock anchors, there is a need to increase knowledge on the stress distribution and failure mechanisms of the rock mass around rock anchors.

The failure mechanisms of rock anchors have been investigated formerly in the laboratory to some extent. Failure mode 3 has been well tested in the laboratory, for example by Barley (1997), Kim and Lee (2005), Ivanovic and Neilson (2008) and Akisanya and Ivanovic (2014). For the more uncertain failure modes 1 and 2 testing have not been performed to the same degree in the laboratory. The mentioned Barley (1997) also tested failure mode 2 as well and failure mode 1 has been tested on intact rock blocks by García-Wolfrum et al. (2007) with anchors of small dimension (up to 10 cm length), which showed that the failure surface was not conical but expanding towards the surface. Dados (1984) and Grindheim et al. (2022) tested failure mode 1 on block models with aluminium and concrete blocks, respectively. The tests by Dados (1984) showed that the blocks close to the anchor bulged upward and the vertical joints tended to open when the anchor was pulled upward. Grindheim et al. (2022) showed that load arches are induced in each layer of a laminar block model when pushed upward, which increased the block model capacity compared to the estimated anchor capacity with the current design methods.

The ground rock mass contains fractures, geological discontinuities and foliation that may function as weakness planes. These discontinuities divide the rock into blocks of various sizes. In such blocky rock masses, the failure often occurs along the geological structures (Grindheim et al., 2022). Grindheim et al. (2022) demonstrated that load-arching is induced in a blocky and laminar block model under a concentrated load, which enhanced the capacity of the block model. These tests only tested one type of block pattern with continuous horizontal joints and discontinuous vertical joints. It is therefore important to investigate how the load is transferred from an anchor to blocky rock masses with varying block patterns as well as the load capacity of the different block patterns.

This paper is a continuation of the work by Grindheim et al. (2022). The paper investigates the deformation behaviour of blocks set in different patterns and the failure mode of the patterns through laboratory pull tests on a specially designed test rig. The effect changes in the block pattern and stress conditions have on the arching effect and model capacity will also be investigated. All tests were monitored by digital image correlation (DIC) to get the full field displacements in the models.

1. TEST ARRANGEMENT AND PROCEDURE

1.1. Test setups

A specially developed laboratory rig was built to test the load distribution and failure pattern of several block models with varying joint patterns, the test setups are shown in Figure 2. The test rig consisted of a steel frame with inner dimensions of 223 × 153 × 30 cm (width × height × depth). Inside the steel frame, there is 10 hydraulic cylinders fastened on the left inner vertical wall and 16 hydraulic cylinders fastened on the top horizontal wall, which can provide horizontal and vertical stress, respectively. The hydraulic cylinders have a capacity of 142 kN each, 10 cm stroke and there are fastened 3 cm thick steel plates on ball mounts towards the test material. At the bottom centre of the frame, there are fastened two large pistons with a steel block of 10 × 10 × 25 cm (width × height × depth) in between, which represents a rock anchor. The steel block will from now on be termed anchor. The pistons around the anchor have a capacity of 225 kN each, which results in an anchor capacity of 450 kN. The working area inside the hydraulic cylinders in the frame is 190 × 120 × 30 cm. Inside the working area, the block material is placed which represents a rock mass. The hydraulic system is servo controlled. The movements of the blocks in the model are monitored by digital image correlation (DIC) technology with two cameras. The hydraulic pressure is monitored on the horizontal hydraulic cylinders and the anchor pistons which is used to calculate the horizontal stress and anchor force. The displacement of the anchor pistons is measured by thread extensometers, which also is used for anchor displacement control.

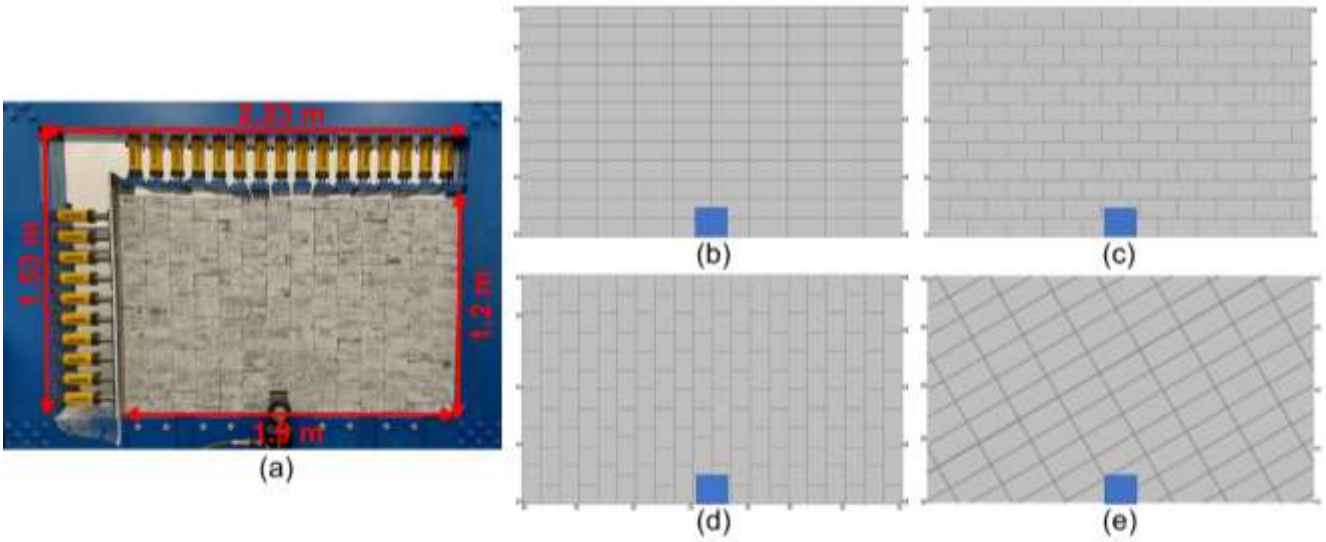

Figure 2. (a) Test setup of the laboratory tests with concrete blocks within the steel frame, the concrete blocks were placed in different patterns as sketched: (b) block pattern 1 - continuous horizontal and vertical joints, (c) block pattern 2 - continuous horizontal and discontinuous vertical joints, (d) block pattern 3 - discontinuous horizontal and continuous vertical joints, and (e) block pattern 4 - 25° tilt on the horizontal and vertical joints.

Monitoring of the tests with DIC cameras required preparation of the blocks. A speckle pattern had to be applied to the blocks on the side facing the cameras. First the blocks were painted white, then the speckle pattern was applied which was non-repetitive 50/50 black and white with high contrast. The size of the speckles should be at least 3-4 pixels to avoid aliasing (Correlated Solutions, 2020). The cameras were placed in line with the outer edges of the concrete blocks at such a distance that the whole model was visible in both cameras, which resulted in an angle of 25.5° in between them. The cameras were set to take 5 images per second in the tests not run to failure and 10 images per second in the failure tests. The images of the tests were analysed with the software Vic-3D (Correlated Solutions, 2020) after the tests. The software calculated the displacements and strains in the models from changes in the speckle pattern by taking reference in an image from the beginning of the test.

The material used in the tests were 27 × 6 × 20 cm concrete pavement blocks. The pavement blocks were cut into smaller blocks of dimensions of 13 × 6 × 19 cm and 6.5 × 6 × 19 cm. Small errors occurred during the cutting of the blocks, which resulted in that not all the layers were in contact with the horizontal hydraulic cylinders. Therefore, to ensure contact between all the layers and the horizontal hydraulic cylinders, cement mortar was casted on the side to fill all the gaps. The cement mortar had a water-cement ratio (W/C) of 0.28.

The material properties of the concrete pavement blocks were found by drilling cores out of the blocks and test them under uniaxial compression as described in Bieniawski and Bernede (1979). The Young's modulus (E) and

Poisson's ratio (v) was calculated from the measured axial and radial strains. The average uniaxial compressive strength (UCS) was measured to 43 MPa, the Young's modulus 23 GPa, and Poisson's ratio 0.22. The density of the concrete was 2272 kg/m^3. The wooden plate was a formwork board with bending strength 58.6 MPa in the longest direction and 42.6 in the shortest direction.

The creation of block pattern 4 with tilted layers, Figure 2(d), required getting the tilt angle correct on the bottom of the frame. The diamond cutters used to cut the concrete blocks at the laboratory were not precise enough to get the right angle from the beginning. Therefore, the first layer in the tilted model were made from wood since the saw was more precise and easier to work with.

1.2. Test procedure

Multiple tests of the four block patterns (Figure 2) have been done in the test rig. On each of the block patterns, the wall height, vertical stress, and confinement has been varied. All the tests followed the same procedure, which is shown step by step here:

1. The blocks were placed in the frame with the wanted block pattern and height.
2. The left side of the model was evened out with cementitious grout and a wooden plate, the grout was left to harden for a week.
3. The wanted horizontal stress was applied to the blocks from the horizontal cylinders and then the valves were closed, to keep the model from deforming horizontally.
4. A vertical stress was applied to the blocks from the vertical cylinders if a height higher than 1.2 m were to be simulated. The valves were left open to keep the stress constant and let the model deform vertically.
5. If the tests were not run to failure a displacement limit of 25 mm was set on the system.
6. The DIC capturing was started.
7. The blocks were then loaded with a displacement rate of 0.5 mm/s with a force limit. The force limit was increased with 10 kN increments if the movement stopped. For the tests not run to failure, the test was stopped if a force of 50 kN was reached and the movement stopped, or the displacement reached the limit of 25 mm. The failure tests were run to the end of the stroke of the pistons.
8. The anchor was then unloaded slowly.
9. The DIC capturing was stopped.
10. The confining stresses were then removed.

2. RESULTS AND ANALYSIS

A total of 80 tests has been done in the testing rig. These tests have been done on the four block patterns shown in Figure 2. On each block pattern 20 tests without failure were done, except for block pattern 4 where only 16 tests were done, the results from these tests are presented in Tables 1-4. The last test on each block pattern was a failure test.

The test results from block pattern 1 with continuous joints horizontally and vertically are shown in Table 1. The tests shows that the load capacity of the block model is lowest when the height and horizontal stress are at a minimum. The block model capacity increased with increasing wall height and increasing horizontal stress.

Table 1. Results from the non-failure tests of block pattern 1. The colours indicate which tests was stopped by displacement (yellow) and load (green).

		Height (m)				
		0.6	0.9	1.2	4	8
Horizontal stress (MPa)	0	Load 11.7 kN Disp. 25.2 mm	Load 16.1 kN Disp. 25.1 mm	Load 27.1 kN Disp. 25.1 mm	Load 45.1 kN Disp. 25.1 mm	Load 47.8 kN Disp. 18.5 mm
	0.1	Load 14.9 kN Disp. 25.1 mm	Load 19.6 kN Disp. 25.1 mm	Load 33.3 kN Disp. 25.1 mm	Load 44.4 kN Disp. 25.1 mm	Load 47.0 kN Disp. 12.5 mm
	0.5	Load 20.4 kN Disp. 25.1 mm	Load 31.7 kN Disp. 25.1 mm	Load 46.3 kN Disp. 18.5 mm	Load 46.1 kN Disp. 13.3 mm	Load 48.9 kN Disp. 10.0 mm
	1	Load 23.6 kN Disp. 25.0 mm	Load 38.7 kN Disp. 25.2 mm	Load 46.0 kN Disp. 11.2 mm	Load 48.9 kN Disp. 9.6 mm	Load 49.0 kN Disp. 8.9 mm

The results from the tests on block pattern 2 with continuous horizontal joints and discontinuous vertical joints are shown in Table 2. The tests show similar results as for block pattern 1, that the load capacity of the block model

is lowest when the height and horizontal stress are at a minimum. The block model capacity increased with increasing wall height and increasing horizontal stress.

Table 2. Results from the non-failure tests of block pattern 2. The colours indicate which tests was stopped by displacement (yellow) and load (green).

		Height (m)				
		0.6	0.9	1.2	4	8
Horizontal stress (MPa)	0	Load 14.1 kN Disp. 25.2 mm	Load 18.9 kN Disp. 25.1 mm	Load 16.3 kN Disp. 25.3 mm	Load 38.9 kN Disp. 25.2 mm	Load 43.0 kN Disp. 6.8 mm
	0.1	Load 15.3 kN Disp. 25.0 mm	Load 20.5 kN Disp. 25.3 mm	Load 26.7 kN Disp. 25.1 mm	Load 43.1 kN Disp. 25.1 mm	Load 47.4 kN Disp. 5.8 mm
	0.5	Load 20.3 kN Disp. 25.1 mm	Load 31.4 kN Disp. 25.1 mm	Load 44.7 kN Disp. 23.1 mm	Load 45.5 kN Disp. 11.7 mm	Load 47.8 kN Disp. 5.0 mm
	1	Load 23.4 kN Disp. 25.1 mm	Load 40.4 kN Disp. 25.1 mm	Load 44.3 kN Disp. 12.6 mm	Load 45.5 kN Disp. 8.1 mm	Load 49.9 kN Disp. 4.9 mm

Table 3 shows the results from the tests on block pattern 3 with discontinuous horizontal joints and continuous vertical joints. The tests show similar results as for the first two block patterns, that the load capacity of the block model is lowest when the height and horizontal stress are at a minimum. The block model capacity increased slightly with increasing wall height. The load capacity of block pattern 3 were much more sensitive to the increase in horizontal stress and the load capacity increased considerably with increasing horizontal stress.

Table 3. Results from the non-failure tests of block pattern 3. The colours indicate which tests was stopped by displacement (yellow) and load (green).

		Height (m)				
		0.6	0.9	1.2	4	8
Horizontal stress (MPa)	0	Load 12.9 kN Disp. 25.2 mm	Load 13.0 kN Disp. 25.3 mm	Load 15.0 kN Disp. 25.4 mm	Load 22.7 kN Disp. 25.2 mm	Load 29.6 kN Disp. 25.1 mm
	0.1	Load 21.3 kN Disp. 25.2 mm	Load 39.4 kN Disp. 25.3 mm	Load 40.8 kN Disp. 25.1 mm	Load 46.2 kN Disp. 25.1 mm	Load 42.6 kN Disp. 25.2 mm
	0.5	Load 39.7 kN Disp. 25.2 mm	Load 47.0 kN Disp. 3.6 mm	Load 50.2 kN Disp. 4.6 mm	Load 49.2 kN Disp. 2.6 mm	Load 47.6 kN Disp. 3.0 mm
	1	Load 47.8 kN Disp. 5.3 mm	Load 46.0 kN Disp. 1.1 mm	Load 48.1 kN Disp. 1.3 mm	Load 46.7 kN Disp. 1.5 mm	Load 48.1 kN Disp. 1.3 mm

The final block pattern tested was block pattern 4 with a tilt angle of 25°. The results from this block pattern are shown in Table 4. The tests show similar results as for the other block patterns, that the load capacity of the block model is lowest when the height and horizontal stress are at a minimum. The block model capacity increased slightly with increasing horizontal stress, the test with the lowest heights collapsed with the high horizontal stress and they could therefore not be done. The load capacity of block pattern 4 were much more sensitive to the increase in wall height and the load capacity increased considerably with increasing wall height.

Table 4. Results from non-failure tests of block pattern 4. The colours indicate which tests was stopped by displacement (yellow) and load (green).

		Height (m)				
		0.6	0.9	1.2	4	8
Horizontal stress (MPa)	0	Load 14.1 kN Disp. 25.5 mm	Load 16.6 kN Disp. 25.1 mm	Load 21.1 kN Disp. 25.1 mm	Load 45.2 kN Disp. 14.3 mm	Load 45.5 kN Disp. 3.9 mm
	0.1	Load 14.0 kN Disp. 25.3 mm	Load 15.3 kN Disp. 25.2 mm	Load 24.1 kN Disp. 25.1 mm	Load 45.4 kN Disp. 12.2 mm	Load 46.3 kN Disp. 3.5 mm
	0.5	-	-	Load 36.0 kN Disp. 25.1 mm	Load 46.4 kN Disp. 6.5 mm	Load 47.4 kN Disp. 2.5 mm
	1	-	-	Load 46.3 kN Disp. 18.7 mm	Load 46.6 kN Disp. 7.5 mm	Load 45.5 kN Disp. 2.0 mm

The displacement patterns of the different block models from the DIC measurements are shown in Figures 3-6. These are shown at the maximum displacement for the same loading condition for each block pattern. The loading

condition is height 1.2 m and horizontal stress 1 MPa. For block pattern 1, a loading condition of height 1.2 m and horizontal stress 0.1 MPa is included to show the effect of the horizontal stress. The increase in horizontal stress reduced the vertical displacement towards the top of the block model for block patterns 1-3. While the increased horizontal stress led to a concentrated vertical displacement along or normal to the joints for the tilted block pattern 4 (Figure 6).

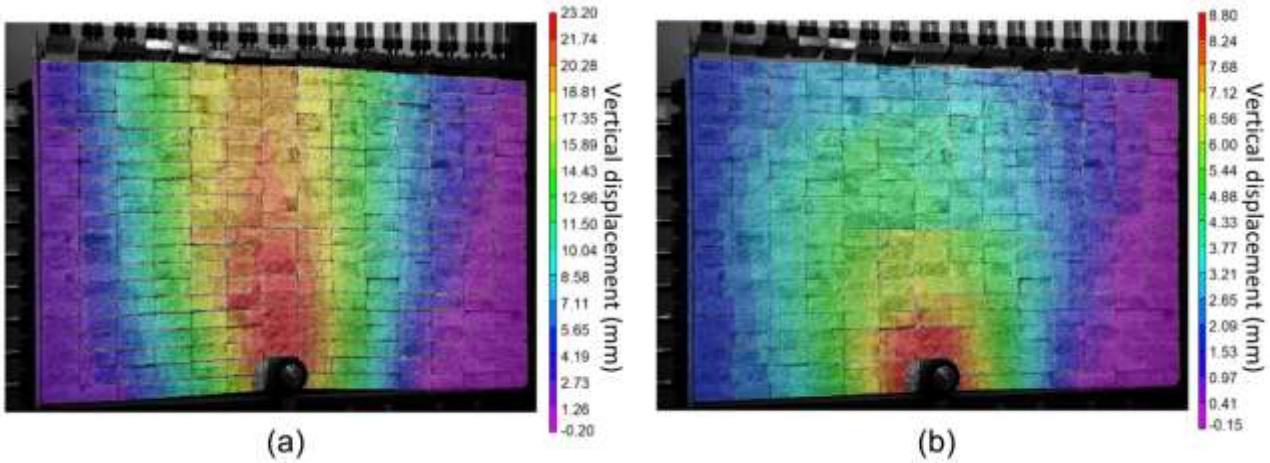

Figure 3. Vertical displacement pattern of two tests of block pattern 1: (a) height 1.2 m, horizontal stress 0.1 MPa; and (b) height 1.2 m, horizontal stress 1 MPa.

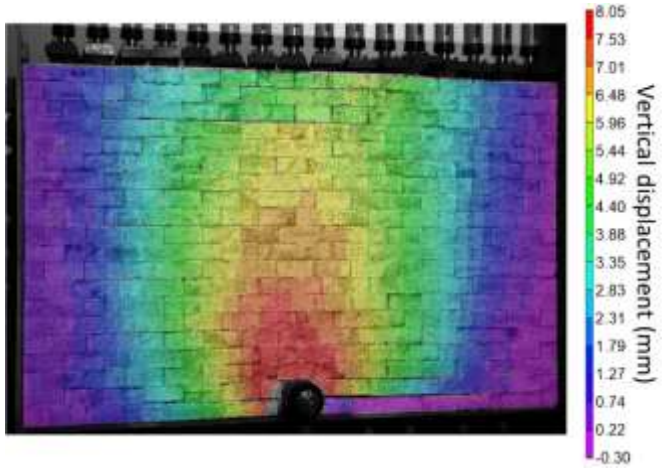

Figure 4. Vertical displacement pattern of block pattern 2 with height 1.2 m and horizontal stress 1 MPa.

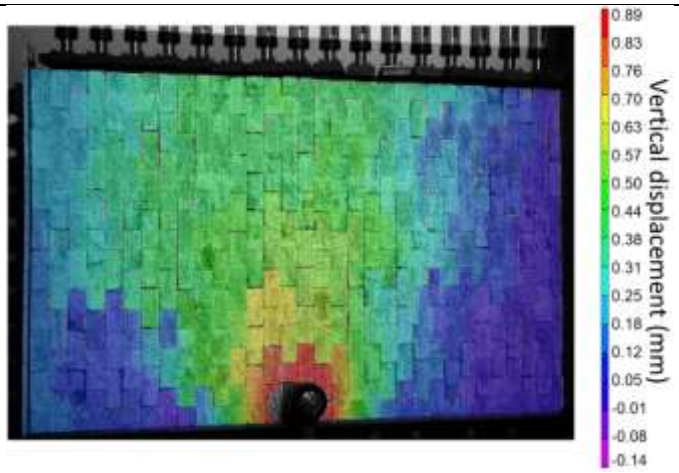

Figure 5. Vertical displacement pattern of block pattern 3 with height 1.2 m and horizontal stress 1 MPa.

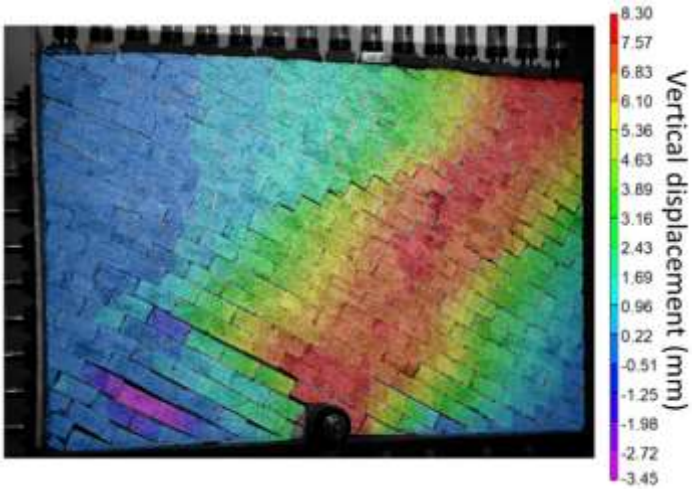

Figure 6. Vertical displacement pattern of block pattern 4 with height 1.2 m and horizontal stress 1 MPa.

Figure 7 shows the horizontal stress against time for the tests with 1.2 m height and 0.1 MPa applied horizontal stress. The plots show a slight decrease in the horizontal stress at the beginning after the cylinders were closed at the wanted stress level, this is likely due to some small leakages of oil in the cylinders. When load is applied to the anchor, the horizontal stress increases above the applied stress level in the models with block patterns 1-3 while it decreases in the model with block pattern 4. The increase in horizontal stress is highest for block patterns 1 and 2, these reached the same level of 0.31 MPa. The increase in horizontal stress in the models indicate that load arches are formed in the block models as described by Grindheim et al. (2022). The load arches increase the horizontal stress by 2-3 times. In the model with tilted blocks, the horizontal stress decreased when anchor load was applied.

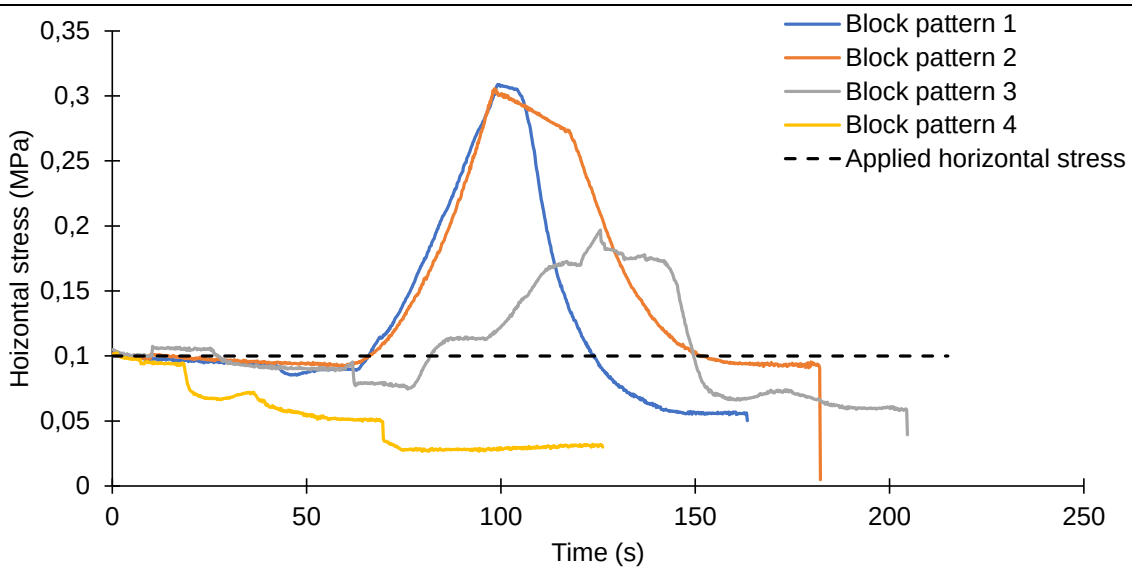

Figure 7. The average horizontal stress from the tests with 1.2 m height and 0.1 MPa applied horizontal stress of all the block patterns. The dashed line shows the applied horizontal stress at the beginning of the tests.

The block patterns were run to complete failure in the last test for each of them, the failures are shown in Figure 8. The failure tests were run with block model heights of 0.9m and horizontal stress of 0.5 MPa, for block model 4 the horizontal stress was reduced to 0.1 MPa since this block pattern gave in with a horizontal stress of 0.5 MPa. All the tests failed as an inverted cone and the fracturing followed the block patterns in all the failure tests. The apex angle of the failure cones varied from 90° -140°. The maximum load capacity of each of the block patterns were 29.71 kN for block pattern 1, 33.92 kN for block pattern 2, 75.15 kN for block pattern 3, and 19.35 kN for block pattern 4.

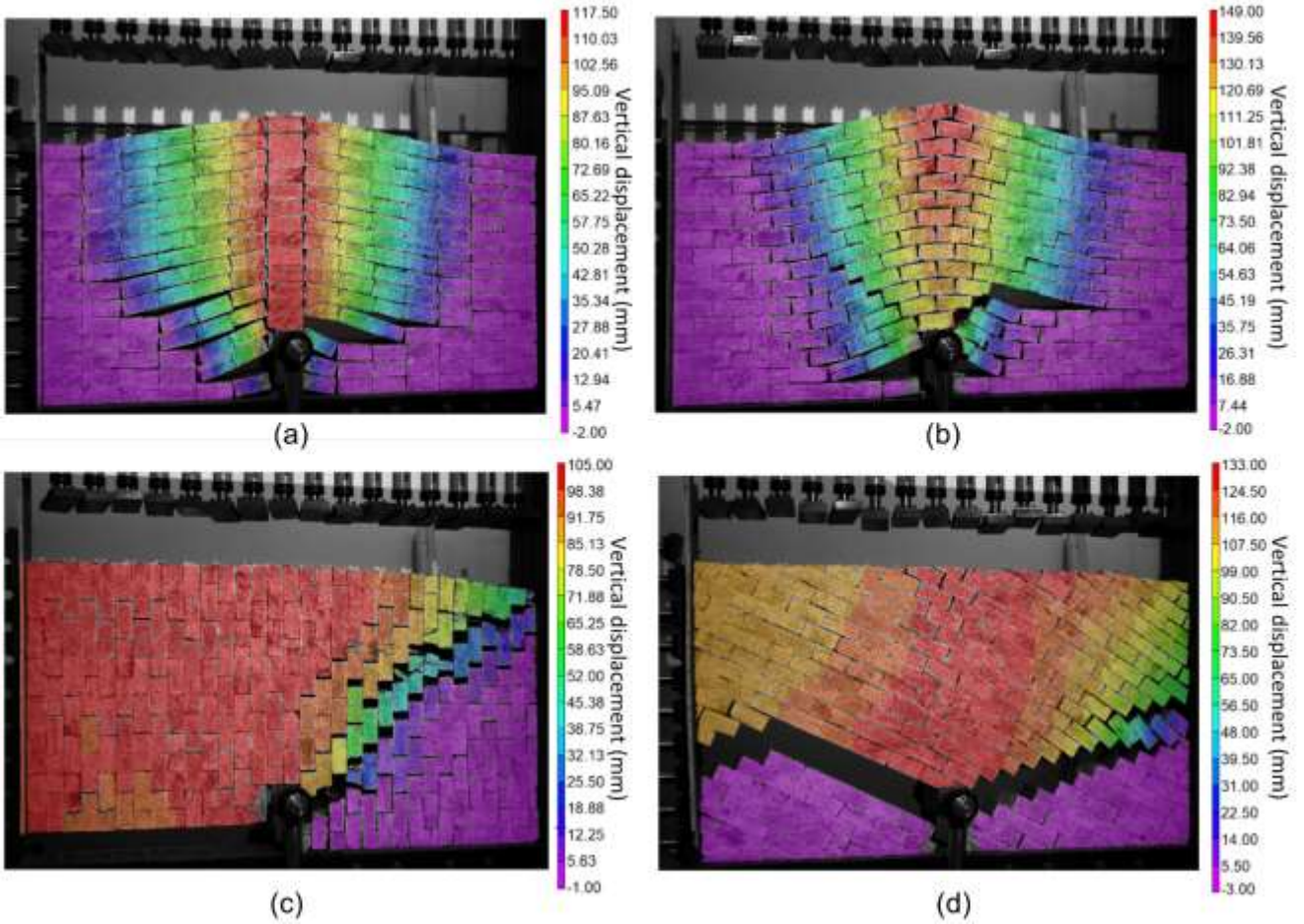

Figure 8. Failure of (a) block pattern 1 with an apex angle of 120^o, (b) block pattern 2 with an apex angle of 100^o, (c) block pattern 3 with an apex angle of 90^o, and (d) block pattern 4 with an apex angle of 140^o.

3. DISCUSSION

The laboratory tests aimed to develop a better understanding of how joint patterns in a rock mass affects the uplift failure around a rock anchor, failure mode 1 in Figure 1, through block models. The tests showed that the joint patterns had a visible effect on the vertical displacement in the block models with the same boundary conditions, shown in Figures 3-6. The displacement in the block models were greatest in the directions parallel or normal to the joints, which became evident with tilted pattern in Figure 6. The in-situ stresses also influenced the rock mass displacements, see Tables 1-4. In block pattern 3 the anchor capacity decreased with increasing vertical stress when the horizontal stress was low (see 4 and 8 m depth in Table 3) but not zero. The joint patterns also affected the failure shape. The failures followed the joints in the block model (Figure 8), and therefore the apex angles are also dependent on the joints.

The tests looked at the effect of in-situ stresses on the rock mass capacity by changing the boundary conditions on the block models, which is summarised in Tables 1-4. In general, the block model capacity increased with increasing wall height or increasing horizontal stress. For the individual joint patterns, the effect of the height and confinement varied. The capacity of the block models increased the most if the stresses normal to the longest axis of the blocks were increased. This can be transferred to in-situ rock masses, the rock mass capacity is high if the stresses in the rock mass are high and normal to the joint set with the shortest spacing, and the rock mass capacity is low when the stresses in the rock mass are low. In the failure tests, it was evident that block model 3 with the blocks oriented normal to the horizontal stress had the highest capacity.

The block model capacity of the failure tests was estimated with the current design method with the weight of overlying rock (Brown, 2015) and with a shear strength of 100 kPa along a failure surface with an apex angle of

80° from presumptive values given in NPRA (2018) for a rock mass with two joint sets. These gave a block model capacity of 3.8 kN and 26.2 kN for the weight force and presumptive shear strength, respectively, for a block model of height 0.9 m. The weight force is conservative by one order of magnitude from the measured capacities at the end of section 3. The presumptive shear strength is close to the measured capacities of block patterns 1, 2 and 4, while it is only one third of the capacity measured for block pattern 3.

A small-scale block model by Grindheim et al. (2015) showed that load arches are induced in a block model with continuous horizontal and discontinuous vertical joints. Figure 7 shows the horizontal stress development in the tests with 1.2 m height and 0.1 MPa applied horizontal stress. The horizontal stress increased in block models 1-3, which indicates that load arches were formed. The plots demonstrate that the joint patterns influence the development of load arches in the block model. Load arches are formed in the block models with horizontal and vertical joints, while for the block model with tilted joints there is no increase in horizontal stress, which indicate that no load arch is induced. This indicate that an unfavourable joint pattern in a rock mass may lead to no load arch being formed. It also possible that the load arch was formed in this model between the vertical cylinders and the right wall of the frame, but this was not captured as there were no stress measurement on the individual vertical cylinders and on the right wall.

In literature, the apex angle of the failure cone is assumed to be 60-90° depending on the rock mass strength (Littlejohn and Bruce, 1977; Brown, 2015). The apex angle is assumed to be 60° in weak rock masses and 90° in strong rock masses. The failure tests of the block patterns here had apex angles ranging from 90-140°, which is mostly higher than in literature. It was also the test with the highest capacity that had the smallest apex angle, block pattern 3. These tests indicate that the size of the apex angle is dependent on the joint pattern and not the rock mass strength, and that the failure cone follows the joints, as seen in Figure 8.

4. CONCLUSIONS

A total of 80 two-dimensional block model tests were carried out in the laboratory to investigate load arching, the load capacity, and failure of different rock masses. The tests showed increased horizontal stress (i.e., load arching) in the tests with horizontal and vertical joints, while it decreased in the test with a 25° tilt of the joints. The vertical displacement in the block models was greatest in the direction normal to or parallel to the joint sets. The load capacity of the block models increased with both increasing horizontal stress and increasing wall height (corresponding to an increase in depth). The joint patterns affected the load capacity of the models. The failure shape was affected by the joint patterns, the failure surface followed the joint pattern in all the failure tests. The apex angle of the inverted cone was larger than in literature for most of the tests and it was dependent on the joint patterns rather than the rock mass strength.

5. FURTHER RESEARCH

These tests described and discussed here have only used one kind of blocks. In the future, it is necessary to test blocks of different sizes and materials to see how they affect the capacity, deformations, and stresses in the block models. The results should also be transferred to real scenarios, which can be done through numerical models calibrated on these test results. The numerical models can also be used to test the effect of different materials through sensitivity analysis.

6. ACKNOWLEDGEMENTS

The authors acknowledge the financial support of the Research Council of Norway through the research project ROCARC, project number 303448. The partners of the project are NTNU, Norwegian Association of Rock Mechanics (NBG), SINTEF, NGI, The Arctic University of Norway (UiT), Norwegian Public Roads Administration (NPRA), Multiconsult AS, Norconsult AS and NORSAR. The authors thank Gunnar Vistnes, Jon Runar Drotninghaug, Noralf Vedvik, and Torkjell Breivik for their technical assistance in manufacturing and Brage Angell for his participation in the tests.

REFERENCES

Akisanya, A.R., Ivanovic, A., 2014. Debonding along the fixed anchor length of a ground anchorage. Engineering Structures 74, 23–31. DOI: doi.org/10.1016/j.engstruct.2014.05.013.

Aoki, K., 2007. Design and construction of large rock caverns supported by ground anchorages, in: Ground Anchorages and Anchored Structures in Service, Proceedings of the International Conference, Thomas Telford Publishing, London, England. pp. 188–198.

Barley, A.D., 1997. Properties of anchor grouts in a confined state, in: Ground Anchorages and Anchored Structures: Proceedings of the International Conference, Thomas Telford Publishing, London, England. pp. 371–383.

Bieniawski, Z., Bernede, M., 1979. Suggested methods for determining the uniaxial compressive strength and deformability of rock materials. International Journal of Rock Mechanics and Mining Sciences & Geomechanics Abstracts 16, 137–140. DOI: doi.org/10.1016/0148-9062(79)91451-7.

Brown, E.T., 2015. Rock engineering design of post-tensioned anchors for dams - a review. Journal of Rock Mechanics and Geotechnical Engineering 7, 1–13. DOI: doi.org/10.1016/j.jrmge.2014.08.001.

Choi, S.W., Lee, J., Kim, J.M., Park, H.S., 2013. Design and application of a field sensing system for ground anchors in slopes. Sensors 13, 3739–3752. DOI: doi.org/10.3390/s130303739.

Correlated Solutions, 2020. Vic-3D v7 Testing Guide. Correlated Solutions.

Dados, A.T., 1984. Design of anchors in horizontally jointed rocks. Journal of Geotechnical Engineering 110, 1637–1647. DOI: doi.org/10.1061/(ASCE)0733-9410(1984)110:11(1637).

García-Wolfrum, S., Serrano, A., Olalla, C., 2007. Model failure tests on rock anchors, in: 11th Congress of the International Society for Rock Mechanics: The Second Half Century of Rock Mechanics, Taylor & Francis Group, Lisbon, Portugal. pp. 339–342.

Grindheim, B., Aasbø, K.S., Høien, A.H., Li, C.C., 2022. Small block model tests for the behaviour of a blocky rock mass under a concentrated rock anchor load. Geotechnical and Geological Engineering 40, 5813-5830. DOI: doi.org/10.1007/s10706-022-02251-1.

Ivanovic, A., Neilson, R.D., 2008. Modelling of debonding along the fixed anchor length. International Journal of Rock Mechanics & Mining Sciences 46, 699–707. DOI: doi.org/10.1016/j.ijrmms.2008.09.008.

Jordan, L., 2007. Monitoring of multi-strand ground anchors at the City of Manchester Stadium, in: Ground Anchorages and Anchored Structures in Service, Proceedings of the International Conference, Thomas Telford Publishing, London, England. pp. 99–110.

Kim, D.H., Lee, S.R., 2005. Uplift capacity of fixed shallow anchors subjected to vertical loading in rock. International Journal of Offshore and Polar Engineering 15, 312–320.

Koca, M.Y., Kincal, C., Arslan, A.T., Yilmaz, H.R., 2011. Anchor application in Karatepe andesite rock slope, Izmir - Türkiye. International Journal of Rock Mechanics & Mining Sciences 48, 245–258. DOI: doi.org/10.1016/j.ijrmms.2010.11.006.

Littlejohn, G.S., Bruce, D.A., 1977. Rock anchors - state of the art. Foundation publications LTD., Brentwood, Essex, England.

Merrifield, C., Møller, O., Simpson, B., Farrell, E., 2013. European practice in ground anchor design related to the framework of EC7, in: Proceedings of the 18th International conference on soil mechanics and geotechnical engineering: challenges and innovations in geotechnics, Paris: Presses des Ponts, Paris, France. pp. 1835–1838.

Mothersille, D., Littlejohn, S., 2012. Grouting of anchors to resist hydrostatic uplift at Burnley tunnel, Melbourne, Australia, in: Proceedings of the Fourth International Conference on Grouting and Deep Mixing, American Society of Civil Engineers, New Orleans, Louisiana, USA. pp. 1073– 1084.

NPRA, 2018. Handbook V220 – Geotechnics in road construction (in Norwegian). Norwegian Public Roads Administration (Statens vegvesen), Oslo, Norway.

Roesen, B.S., Trankjær, H., 2021. Permanent uplift anchors in Copenhagen limestone, in: IOP Conference Series: Earth and Environmental Science 710, IOP Publishing, Helsinki, Finland. p. 10.

Schlotfeldt, P., Panton, B., Humphries, R., Elmo, D., 2013. New Park Bridge, Kicking Horse Canyon; pier 5 - a difficult foundation on rock, in: 47th US Rock Mechanics/ Geomechanics Symposium, American Rock Mechanics Association, San Francisco, California, USA. p. 8.

Shabanimashcool, M., Olsson, R., Valstad, T., Lande, E.J., Berzins, A., Tuominen, K., Lapsins, J., 2018. Numerical modelling of anchored foundation for wind turbine generators, WTG (in Norwegian), in: Fjellsprengningsdagen - Bergmekanikkdagen - Geoteknikkdagen, NFF, NBG, NGF, Oslo, Norway. pp. 18.1–18.24.

Showkati, A., Maarefvand, P., Hassani, H., 2015. Stress induced by posttensioned anchor in jointed rock mass. Journal of Central South University 22, 1463–1476. DOI: doi.org/10.1007/s11771-015-2664-x.